Passive Radar Distributed Sensor Network for Detecting Silent Aerial and Maritime Targets in Coastal Waters

M.P. Jarabo-Amores, D. Mata-Moya, N. Rey-Maestre,
P.J. Gómez-del-Hoyo and J. Rosado-Sanz
Signal Theory and Communications Department, Polytechnic School, University of Alcalá
Ctra. Madrid-Barcelona km. 33,600. CP. 28805 – Alcalá de Henares, Madrid
SPAIN

mpilar.jarabo@uah .es

ABSTRACT

Passive Radars (PR) are promising emerging technologies to reinforce public security and national defence, and could be complement solutions to protect critical infrastructures and borders. In this paper, a sensor network based on independent PR nodes is presented for monitoring a coastal border scenario. The feasibility of deploying the PR sensors network for border surveillance is studied by means of complete coverage analysis. Electromagnetic simulators are used to include the specific radar scenario characteristics and the bistatic radar cross section modeling of aerial and maritime military targets. Simulation results are validated with real radar data in a selected coastal scenario. Detection and tracking of different targets are carried out: a cooperative DJI Phantom 3 drone, ships and aircrafts landing Rota military airport. Results confirm the feasibility of DVB-T based PRs for monitoring border coastal scenarios.

1.0 INTRODUCTION

Passive Radars (PRs) are promising emerging technologies to reinforce public security and national defence, and could be complement solutions to protect critical infrastructures and borders. In this paper, a sensor network based on independent PR nodes is presented as a novel solution for monitoring large coastal areas due to its lower deployment and maintenance costs. Based on the detection capabilities provided by a PR sensor in a military border coastal scenario including the Rota naval base and the Torregorda Test Center belong to the Spanish National Institute of Aerospace Technique (INTA), a network for covering a large coastline is designed. PR coverage studies are presented for monitoring moving targets in this coastal environment.

System coverage is defined for specific target and interference models, as the maximum range where a target is detected fulfilling the probability of detection and probability of false alarm requirements. In the case study, estimated coverage maps are generated taking into account the Iluminators of Oportunity (IoOs) transmitted powers and antenna features, the PR sensitivity, the excess propagation losses and the target Bistatic Radar Cross Section (BRCS). According to the selected scenario, the following target of interest are defined: medium and high size ships, aircrafts and small-size drones. Different target altitudes relative to ground level are considered for coverage analysis of the aerial targets of interest.

The sensitivity of the PR system, defined as the minimum received power level to fulfil detection requirements, has been calculated using data from the reception chains of IDEPAR, a DVB-T based PR developed by the University of Alcalá [1], [2]. The modelling of excess propagation losses and target BRCS has been performed using electromagnetic simulators: WinProp (AWE Communications GmbH) [3] software, and Ansys HFSS electromagnetic simulator [4] respectively.

For validation purposes, IDEPAR demonstrator was deployed in the facilities of the 11th Aircraft Squadron of the Spanish Navy located in Cádiz (Spain). Detection and tracking of different targets are carried out: a

cooperative DJI Phantom 3 drone, ships with AIS data and aircrafts landing Rota military airport. Results confirm the feasibility of DVB-T based PRs for monitoring large coastal scenarios.

2.0 PASSIVE RADAR OPERATIVE PRINCIPLE

The PR operation is based on a set of techniques to detect targets and to estimate parameters using non-cooperative signals (broadcast, communications, radar, or radio-navigation signals) as IoO, rather than a dedicated transmitter [5], [6]. Due to the absence of a dedicated transmitter, PRs are promising candidates to complement active ones in security and defence applications and are under intensive research [7], [8], [9], [10].

A PR is a multi-static system that allows multiple configurations depending on the number of IoOs and receivers. Due to the lack of control over the IoO, usually two kind of channels are used (Figure 1): a reference one to acquire the IoOs signal, and a surveillance one to capture target echoes from the Area of Interest (AoI). To estimate target dynamic information, delay and Doppler-shifted copies of the reference signal are correlated with the surveillance one to generate the Cross Ambiguity Function (CAF). Digital Video Broadcasting-Terrestrial (DVB-T) IoO are of great interest due to their higher powers, availability, known position, and channel bandwidth (B≈8 MHz). The use of consecutive channels can be exploited for improving detection and localization of low reflectivity targets.

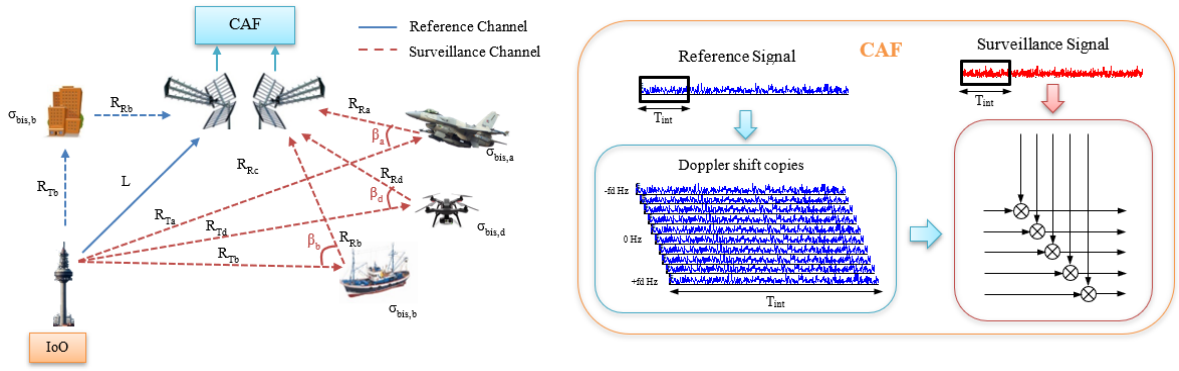

Figure 1: Basic geometry of a PR (left), CAF generation (right). R_{Ti} and R_{Ri} are the target-to IoO and target-to-PR distances; L is the IoO-to-receiver distance, β_i is the bistatic angle, $\sigma_{bis,i}$ is the Bistatic Radar Cross Section (BRCS); i ∈ {b, c, a} refers to building, car, and airplane, respectively. T_{int} is the integration time.

A PR sensor network is composed of multiple PR systems deployed along the radar scenario to increase the radar performances of a single PR system. The PR configuration can be designed to optimize different radar performances: range or velocity resolutions, coverage area, 3D location capabilities… Several strategies can be applied to determine the individual node location depending on the network objectives. In radar literature the Cramér-Rao lower bounds (CRLB) [11], [12] together with the multistatic ambiguity function [13] are exploited to tackle the problem of optimally sensors distribution. In [14], [15] a strategy to dynamical select the pair PR-IoO that produces the best tracking performances of a target moving along a trajectory was addressed. In [16] the problem was studied as a way of improving target resolution in distributed radar systems. Some rules were developed for maximizing target resolution in multiple directions while maintaining high probability of detection. In this work, the nodes physical distribution was determined to maximize the PR coverage area and provide surveillance support to most of the AoI.

3.0 COVERAGE ESTIMATION PROCESS

The key tool for estimating the PR coverage is the bistatic radar equation [6] (1):

$$(R_R R_T)^2 = \frac{p_T \cdot g_T \cdot g_R \cdot \lambda^2 \cdot \sigma_b}{(4\pi)^3 \cdot p_R \cdot l_{IoO-target} \cdot l_{target-PR}} \quad (1)$$

where R_R and R_T are the distances from the target to the passive receiver and from the IoO to the target, respectively. The excess propagation losses associated to both paths are IoO-Target and Target-PR, σ_b is the target's BRCS, and λ is the signal wavelength, p_T is the transmitted power, and g_T and g_R are the gains of the transmitting and receiving antennas, respectively.

When the excess propagation losses are negligible, and the received power is set to the minimum signal required at the input of the RF-front end of the PR, the equation (1) will allow to estimate the Cassini Oval, that is widely used as a first approach for coverage calculations. Nonetheless, there are scenarios, especially those oriented to small targets at low altitudes, where excess propagation losses due will not be negligible, making the Cassini oval estimation very inaccurate. More precise coverage estimations can be achieved using electromagnetic simulators to compute the path excess losses and targets BRCS.

The target BRCS simulation can be directly included in (1), nonetheless, the path losses provided by the electromagnetic simulators usually include the free space losses and the transmitted power, so simulation results are not directly applicable. The PR received power can be obtained from (1), given the received power equation (2), where all the propagation losses have been gathered.

$$p_R = \frac{p_T \cdot g_T \cdot g_R \cdot \lambda^2 \cdot \sigma_b}{(4\pi)^3 \cdot (R_R R_T)^2 \cdot l_{IoO-target} \cdot l_{target-PR}} \quad (2)$$

If terms from the IoO-Target path and Target-PR path are grouped, the power collected by the PR due to the presence of a hypothetical target in a specific position of the area of interest identified by the cartesian coordinates (x,y), can be obtained from (3):

$$\boldsymbol{P}_R(\mathrm{x},\mathrm{y}) = \frac{\boldsymbol{P}_{IoO-Target}(x,y) \cdot \boldsymbol{G}_R(\mathrm{x},\mathrm{y}) \cdot 4\pi \cdot \lambda^2 \cdot \sigma_b}{\boldsymbol{L}_{Target-PR}(x,y)} \quad (3)$$

where $\mathbf{P}_{\text{IoO-Target}}(x,y)$ is the power available at each point off the studied region, considering the transmission characteristics and the full losses from the IoO to the point; $\mathbf{L}_{\text{Target-PR}}(x,y)$ stands for the total losses in the path from the target and the PR location at the same height, and $\mathbf{G}_R(x,y)$ is the reception antenna gain in the target direction. $\mathbf{P}_{\text{IoO-Target}}(x,y)$ and $\mathbf{L}_{\text{Target-PR}}(x,y)$ terms can be obtained through electromagnetic simulation.

The evaluation of (3) produces a PR received power matrix for the selected transmitter configuration, path simulation model and target characteristics. After applying a threshold value determined from the PR sensitivity level, a high accuracy estimated coverage map is obtained.

4.0 IDEPAR DEMONSTRATOR

IDEPAR is a DVB-T based PR demonstrator designed and developed in the University of Alcalá [1], [2]. The acquisition system operates with a bandwidth up to 100MHz. IDEPAR uses a commercial high directivity DVB-T antenna in the reference channel [1], and a seven-element Non-Uniform Lineal Array (NULA) in the surveillance one. The array single element is a prototype antenna with a beamwidth of 84º and a gain of 7,6dBi [17]. The inter-element distances have been estimated using a genetic algorithm to obtain a compromise solution between sidelobe levels and main beamwidth [18].

The NULA configuration allows the design of digital array signal processing techniques. Beamforming techniques are applied at the CAF output [19]. The two-stage processing scheme detailed in [19] is applied to estimate target parameters in the 3D space (range, Doppler, azimuth), Figure 2:

- Firstly, a full-dimensional beam-space based on orthogonal beams in the azimuth coverage area is generated, where a 3D Cell-Averaging Constant False Alarm Rate (CA-CFAR) detector is applied.
- Secondly, Direction of Arrival (DoA) techniques are implemented using a new set of steering angles to increase azimuth estimation accuracy.

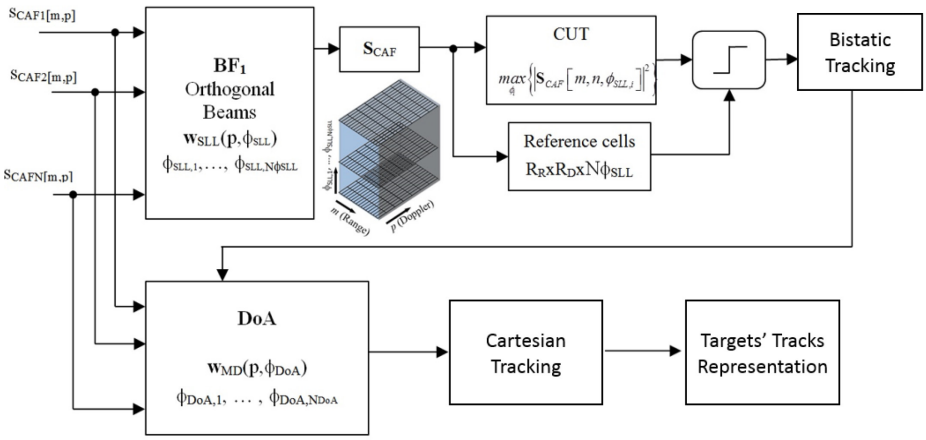

Figure 2: IDEPAR demonstrator tow-stages processing scheme: initial detection with orthogonal beams, second stage of high resolution DoA estimation.

5.0 RADAR SCENARIO

In this work a PR sensor network is proposed to provide maritime and aerial surveillance of a coastal border area in the south of SPAIN. A coastal area including the Rota naval base and the Torregorda Test Center belong to INTA was selected as military border scenario (Figure 3). An area of approximately 150km of coastline with a thickness of at least 20km is defined as AoI. The main objective of the Sensor network is to detect and track maritime and low altitude aerial targets approaching to the military facilities. The following target of interest were defined: medium and high size ships, fighters at low altitudes and small-size drones.

A study of the DVB-T transmitters close to the AoI was carried out and five transmitters were identified (Table 1). Figure 3 presents the IOs location and transmitted beams. Jerez is the main IoO and provides DVB-T broadcasting services to the whole AoI with a higher transmission power. The rest of IoOs are local DVB-T transmitters can be use as illumination sources in the areas close to their own locations.

A PR sensors network composes of 5 nodes was selected. The nodes physical distribution was determined to maximize the PR coverage area and provide surveillance support to most part of the defined AoI. Due to the radar scenario particularities, the sensor network was distributed along the coastline choosing the distance between nodes to overlap the individual coverage areas and provide large maritime surveillance. The nodes physical distribution is presented in Figure 3. The AoI close to the military facilities is covered by 2 PRs due to the proximity of Jerez IoO. Furthermore, three passive radar systems are concentrated in the south part of the AoI where the adverse relief profile and the larger distance from the main IoO can limit the system coverage. Each network node was composed of a complete PR system. The use multiple IoOs as illumination sources for a single node, as well as the connection between different PR nodes that share parts of their surveillance area, allow the design of multistatic PR configurations to increase the target detection and tracking performances and to provide a 3D localization for aerial targets.

Figure 3: Radar sensor network deployment in the radar scenario: AoI (yellow area), IoOs emplacement and radiation pattern near to the AoI (green) and PR along the coastal border (red).

Table 1: DVB-T transmitters information.

	JEREZ	SANLUCAR	CONIL	VEJER	BARBATE
LONGITUDE	-6.15391º	-6.34542º	-6.13985º	-6.01471º	-5.84499º
LATITUDE	36.63603º	36.77999º	36.29547º	36.26480º	36.14430º
EIRP	67.20dBm	53.91dBm	49.19dBm	40.04dBm	49.20dBm

6.0 PASSIVE RADAR NETWORK COVERAGE ANALYSIS

The viability of the proposed PR sensor network was studied by means of the system coverage analysis. In order to cover the whole AoI, a network configuration considering multiple PR-IoO pairs is selected. The Jerez IoO is selected as reference source for all the network nodes, while the rest of IoOs are only considered for the closer PR locations. Table 2 summarises the PR-IoO pairs selected in the PR sensor network. For each PR-IoO pair the excess propagation losses are estimated by means of WinProp electromagnetic simulator. This software allows the selection of different propagation models and the integration of Geographic Information Systems (GIS) data in order to model the relief of the PR scenario. In this work, global digital elevation model version 2 provided by the Advanced Spaceborne Thermal Emission and Reflection Radiometer (ASTER) was selected [20].

Table 2: PR-IO pairs belonging to the designed radar sensor network.

	JEREZ	SANLUCAR	CONIL	VEJER	BARBATE
PR 1	yes	yes	no	no	no
PR 2	yes	yes	yes	no	no
PR 3	yes	no	yes	yes	no
PR 4	yes	no	yes	no	yes
PR 5	yes	no	yes	no	yes

WinProp tool was configured to compute the two different simulation process needed in equation (3) for the PR system coverage estimation, using the Dominant Path Prediction Model (DPM) as full 3D electromagnetic simulation method:

- The power strength produced by IoO in each cell of the radar scenario, $P_{IoO\text{-}Target}(x,y)$.
- The path losses from the PR location to each cell of the radar scenario, $L_{Target\text{-}PR}(x,y)$.

For maritime target a medium altitude of 5m is considered. The aerial targets are modelled as fighters and drones flying at 100 meters form sea level.

6.1 Target BRCS

The target BRCS modelling was carried out using Ansys HFSS [4] with a bistatic angle dependant approach. In this approach, the Bistatic angle, β, was set to a constant value and the estimation process was performed from the target model rotation in the horizontal plane. The following conditions were assumed for the BRCS simulations process:

- Simulations were set up with an incident plane wave impinging on the center of the target.
- Four bistatic angles β are considered: 0 º, 30 º, 60 º and 90 º.
- The target model was rotated in steps of 5 º to generate the target BRCS.

6.1.1 Maritime Targets of Interest

Three military ships of different sizes were selected as representative maritime targets:

- Visby corvette: Swedish Navy corvette with a size of 72.3 x 10.4m^2. It was designed with stealth technology, and the hull is constructed with a PVC, carbon fiber and vinyl laminate.
- Admiral Gorshokov frigate: Russian navy frigate with a size of 132 x 16m^2.
- USS New Jersey battleship: 270x33m^2 size battleship from the United States navy. It was selected as model of big size ship, although it is currently decommissioned.

Figure 4 shows the three targets BRCS estimation results for a bistatic angle β = 0. The BRCS mean values along the selected bistatic angles are summarized in Table 3.

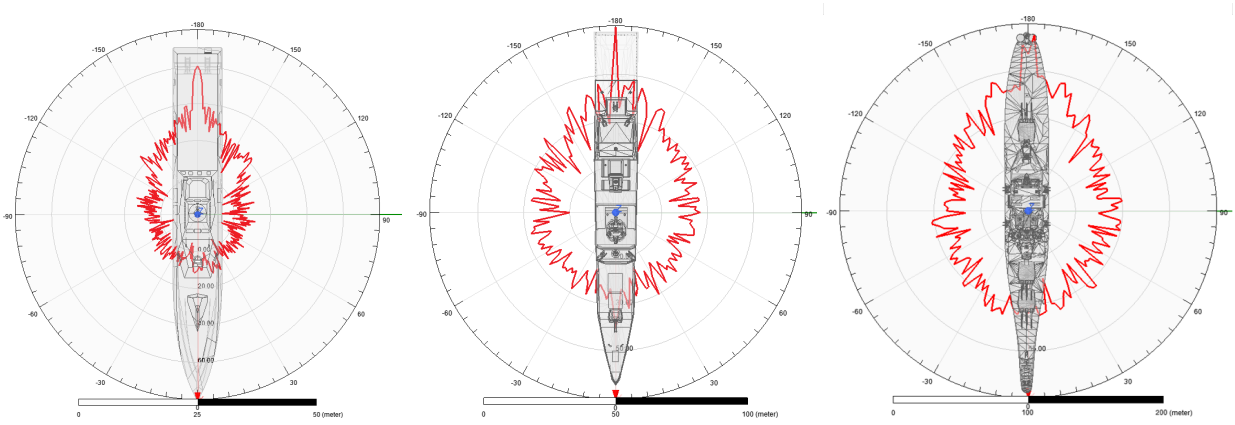

Figure 4: BRCS for a bistatic angle β = 0 for three maritime targets: Visby corvette (left), Admiral Gorshkov frigate (center) and USS New Jersey battleship (right).

Table 3: Maritime target mean BRCS along the considered bistatic angles. The BRCS for coverage analysis is remarked in red.

	β =0	β =30	β =60	β =90
Visby corvette	27.48 dBsm	25.21 dBsm	27.43 dBsm	25.88 dBsm
Admiral Gorshkov frigate	32.08 dBsm	31.35 dBsm	31.34 dBsm	28.95 dBsm
USS New Jersey battleship	50.41dBsm	48.64 dBsm	47.84 dBsm	47.94 dBsm

6.1.2 Aerial Targets of Interest

The aerial targets expected in the radar scenario are small and medium size aircraft flying at low altitude to avoid the active radar systems. A F16 fighter was selected as representative aerial target. The simulation material was set to aluminium due to its high presence in the aircraft structure. As alternative target, a DJI Phantom III was selected to evaluate the system performances in presence small drone. As simulation materials Kevlar was selected for the main body and the blades, copper for the rotors and lithium for the battery. In both cases a flight altitude of 100m from sea level were selected. Figure 5 shows the aerial targets model and their estimated BRCS for a bistatic angle β = 0. The BRCS simulation results for the considered bistatic angles are summarized in Table 4.

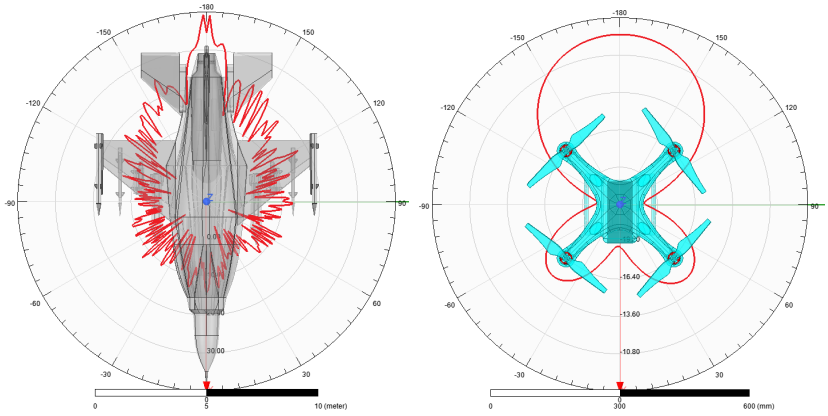

Figure 5: BRCS for a bistatic angle β = 0 for aerial targets: F16 fighter (left), DJI Phantom III drone (right).

Table 4: Aerial target mean BRCS along the considered bistatic angles. The BRCS for coverage analysis is remarked in red.

	β =0	β =30	β =60	β =90
F16 fighter	13.48 dBsm	13.97 dBsm	12.06 dBsm	13.39 dBsm
DJI Phantom III	-11.32 dBsm	-11.25 dBsm	-13.69 dBsm	-12.61 dBsm

6.1.3 Coverage Estimations

The PR sensor network coverage was estimated for the different selected targets considering the PR-IoO pairs described in Table 2. The estimations of the single PR-IoOs pairs were combined to obtain the sensor network coverage area. A system sensitivity of S_{min}=-141.86 was estimated taking into consideration a

Swerling I target model, a probability of detection and false alarm of P_D=80% and $P_{FA}=10^{-5}$ respectively, and the acquisition components of IDEPAR demonstrator.

The coverage estimation results for maritime targets are depicted in Figure 6 (left). Results show a high coverage dependence with the distance from the main IoO, Jerez DVB-T transmitter. Its higher transmitted power allows a large coverage in the closer coastal areas, whereas the lower transmitted power of the rest of IoOs limits the coverage range in the south part of the AoI. This is highlighted in Figure 6 (right) where the IoO that provide a higher SNR in the AoI is depicted. The Jerez transmitter produces a high power in most of the radar scenario, whereas the relevance of the local DVB-T transmitters is enclosed to their surroundings.

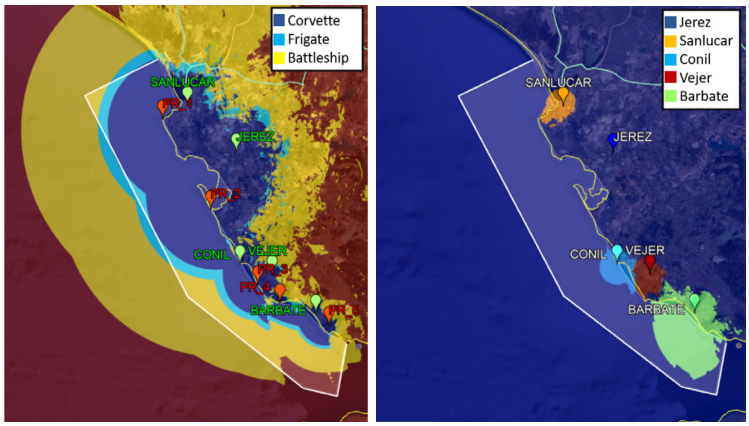

Figure 6: Coverage analysis for maritime targets: estimated coverage (left); IoO that produces a higher SNR at the area of interest (right).

The coverage estimation results for the aerial targets are depicted in Figure 7. The F-16 fighter coverage exceeds almost all the AoI, only a small shadowed area in the south part of the radar scenario is presented. Just as in the maritime targets case, the larger distance to the main IoO the higher coverage restrictions. On the other hand, the drone reduced BRCS drastically affect to the system performance.

The 3D freedom movement of the aerial targets makes insufficient the 2D tracking capabilities provided using linear array based surveillance systems. The multistatic passive radar configurations turn into essential task to provide 3D location and tracking. Figure 7 (right) shows the fighter coverage areas where at least two PR-IoO pairs achieve the detection requirements allowing the implementation of multistatic approaches.

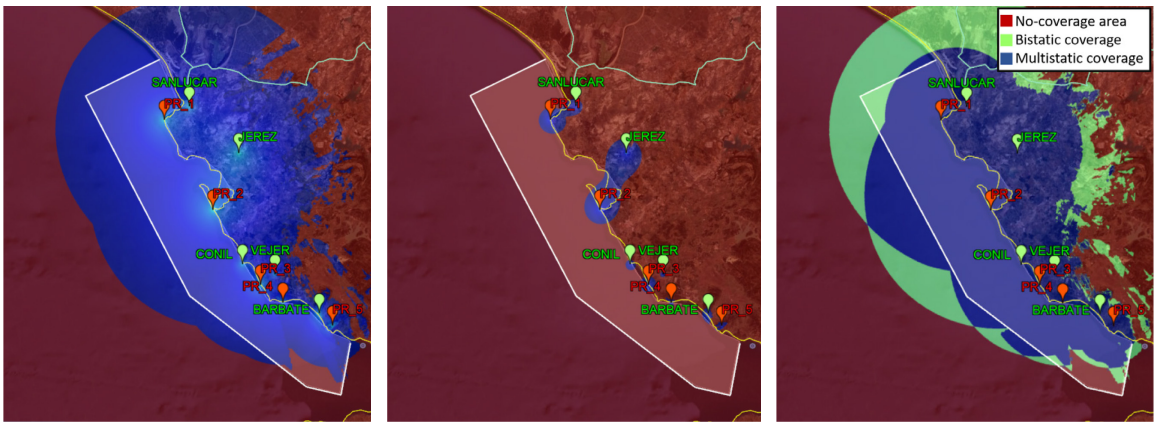

Figure 7: Estimated coverage for the aerial targets: F-16 fighter (left); DJI Phantom III (center); and analysis of the multistatic PR availability (right).

A range coverage estimation for each PR node and type of target was summarized in Table 5. The range coverages are estimated as the distance between the PR and the furthest coverage point along the broadside direction, guaranteeing a continuous coverage.

Table 5: Maximum continuous range coverage for each maritime and aerial target.

	Corvette	Frigate	Battleship	Fighter	Drone
PR 1	20.19km	23.91km	51.7km	39.3km	4.05km
PR 2	20.47km	24.06km	50.41km	40.68km	4.92km
PR 3	10.59km	13.14km	40.51km	27.75km	2.71km
PR 4	5.95km	7.24km	18.6km	21.20km	1.30km
PR 5	7.78km	8.98km	17.4km	15.70km	2.50km

7.0 EXPERIMENTAL RESULTS: REAL DATA ANALYSIS

To validate the proposed PR sensor network, the IDEPAR demonstrator was deployed in the PR location 2 corresponding to the facilities of the 11th Aircraft Squadron of the Spanish Navy. Jerez DVB-T transmitter at 21.3km from the PR location was selected as IoO. IDEPAR was configured to acquire datasets of 40s with a 20MHz continuous bandwidth at a central frequency of 738MHz. For each acquisition and each NULA element of the surveillance channel, 159 CPIs were generated using a PRI = 250ms and a Tint = 500ms. Doppler and range resolutions of 4Hz and 15m, respectively, are obtained. Surveillance signals were pre-processed using interference suppression technique based on the Extensive Cancellation Algorithm [21]. For each CPI and array element, a CAF was generated to apply the two-stage processing scheme.The IDEPAR detection and tracking capabilities were analysed by means of a cooperative small drone. A controlled Phantom III with a GPS device was employed. The flight distance and altitude were limited by the drone operator due to the control system connection coverage and the visual line-of-sight flight mode requirements. Two radar data set were reordered. In the first one, the drone followed an irregular path with different aperture curves and movement directions. The maximum distance reached in this flight was 270m. The second data set comprises an almost radial drone trajectory. The drone flight begins at 340m from the PR reaching a maximum distance from the RP of 400m, where the drone makes an abrupt change of direction to approach quickly to the PR location.

The DoA estimation results for both drone data sets are depicted in Figure 8. Estimated angles close to the GPS data were obtained. The main angle estimation errors are produced by the clutter sources interference during the lower target velocity moments in the tight turns.

Figure 9 shows a google earth view of the drone tracks confirmed by the tracker system and the real target path provided by the GPS data. The estimated tracks stick to the GPS path provided by the cooperative target along the whole trajectories. The higher estimation errors are produced in the beginning of the radial trajectory due to the movement abrupt direction change. Nevertheless, the estimated track quickly converges to the real path.

The detection coverage analysis was carried out using the available non-cooperative moving targets during the measurement campaign. Two non-cooperative targets were selected: one aerial target in the surroundings of the Rota naval base and one maritime targets carrying out the port approach operation.

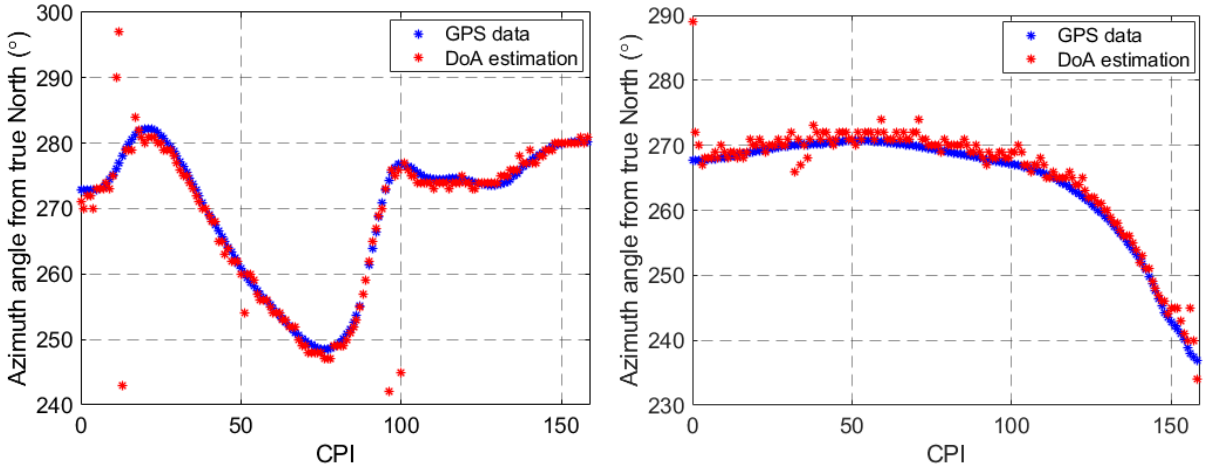

Figure 8: DoA estimation results for a cooperative DJI Phantom III (blue line) and the real target trajectory form the GPS data (white) for two different flying tests.

Figure 9: Tracking results for a cooperative DJI Phantom III (green line) and the real target trajectory from the GPS data (white) for two different flying tests.

Figure 10 (left) shows the aerial and maritime target detection and tracks obtained during measurement campaign. A detailed view of both target is presented in Figure 10 (right). The aircraft was detected at a maximum distance of 28.7 km from the PR during its landing trajectory on the Rota military airport. Due to the large distance to PR and its direct relation with location error applying DoA techniques, the detection points present a large dispersion around the estimated trajectory. Nevertheless, a quasi-straight trajectory pointing to the airport runway is obtained, confirming the aerial detection performances of IDEPAR demonstrator at large distances. Concerning maritime target, the Volcán de Teneguía cargo is detected during its approaching to Cadiz port at 14km from PR location. Three different 40 seconds acquisitions were presented following the maritime target port approach maneuver. The AIS data was employed to generate the real target estimated path during the port approaching maneuver. The PR estimated tracks stick to the AIS trajectory reaching a maximum deviation between AIS and estimated trajectory of 100m, and confirming the maritime target detection and tracking capabilities of IDEPAR demonstrator.

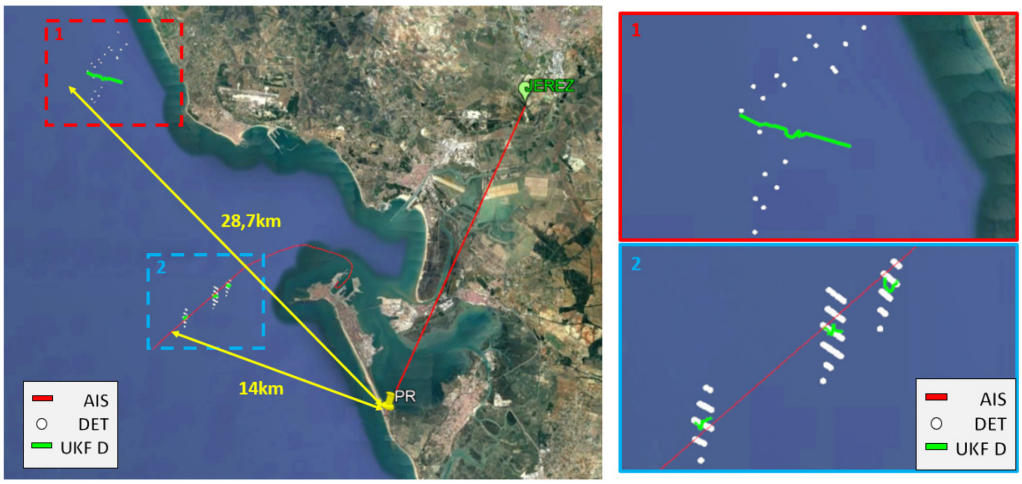

Figure 10: Tracking results for non-cooperative targets: general view of target detections and estimated tracks (left); detailed views of both targets (right): Airplane(1) and ship (2).

8.0 CONCLUSIONS

In this paper the feasibility of the use of a PR sensor network for coastal border control was studied. An area of 150km of coastline with a thickness of at least 20km in the south of Spain was selected as AoI. The area includes the the Rota naval base and the Torregorda Test Center belong to INTA as military protected facilities. A sensor network composed of five PR nodes exploiting five DVB-T transmitters as IOs was designed to maximize the coverage area. The PR sensor viability was studied with theoretical analysis and real radar data acquired in the selected radar scenario.

A theoretical analysis based on system coverage analysis was carried out. Estimated coverage maps were generated taking into account the IoOs transmitted powers and antenna features, the PR sensitivity, the excess propagation losses and the target BRCS. According to the selected scenario, the following target of interest were defined: medium and high size ships, fighters and small-size drones. The exceed propagation loses were computed by Winprop electromagnetic simulator. The targets BRCS was estimated by means of Ansys software considering the target 3D model and construction materials. Coverage results show the viability of a PR sensor network for coastal border control in the selected radar scenario.

To validate the proposed PR sensor network, the University of Alcalá IDEPAR demonstrator, designed for DVB-T signals, was deployed in one of the selected node locations, the facilities of the 11th Aircraft Squadron of the Spanish Navy located in the Torregorda Test Centre, Cádiz (Spain). Detection and tracking of different targets were carried out: a cooperative DJI Phantom 3 drone, a ship with AIS data and an aircraft near to the Rota military airport. Results confirm the feasibility of DVB-T based PRs for monitoring large coastal scenarios.

9.0 REFERENCES

[1] M.P. Jarabo-Amores, J.L. Bárcena-Humanes, P.J. Gómez-del-Hoyo, N. Rey-Maestre. D. Juara-Casero, F.J. Gaitán-Cabañas, D. Mata-Moya. 2016. IDEPAR: a multichannel digital video broadcasting-terrestrial passive radar technological demonstrator in terrestrial radar scenarios. IET Radar, Sonar and Navigation.

[2] N. del Rey-Maestre, D. Mata-Moya, MP. Jarabo-Amores, PJ. Gómez-Hoyo, JL. Bárcena, J. Rosado. 2017. Passive radar array processing with non-uniform linear arrays for ground targets detection and localization. Remote Sensing. 9: 756-785.

[3] WinProp Propagation Modeling: A new dimension of wave propagation and radio network planning. Web: https://altairhyperworks.com/product/feko/winprop-propagation-modeling. Last access March 2020.

[4] ANSYS HFSS, 3D Electromagnetic Field Simulator for RF and Wireless Design. Web: https://www.ansys.com/products/electronics/ansys-hfss. Last access March 2020.

[5] IEEE standard for radar definitions, IEEE Std 686-2017, 2017.

[6] Nicholas J. Willis. 2005. Bistatic Radar. Scitech Publishing.

[7] P. Howland. 2005. Editorial: Passive radar systems. IEE Proceedings – Radar, Sonar and Navigation. 152(3): 105-106.

[8] Farina and H. Kuschel. 2012. Guest editorial special issue on passive radar (part I). IEEE Aerospace and Electronic Systems Magazine. 27(10).

[9] R. Klemm, et al. 2017. Novel Radar Techniques and Applications Volume 1: Real Aperture Array Radar, Imaging radar, and Passive and multistatic radar. The Institution of Engineering and Technology 1.

[10] K.E. Olsen and H. Kuschel. 2017. From the editors of the special issue: Passive and multi-static radar for civil applications. IEEE Aerospace and Electronic Systems Magazine. 32(2).

[11] Cramér, Harald, Mathematical Methods of Statistics, Princeton, NJ: Princeton Univ. Press. ISBN 0-691-08004-6.OCLC 185436716, 1946.

[12] Rao, Calyampudi Radakrishna, Information and the accuracy attainable in the estimation of statistical parameters, Bulletin of the Calcutta Mathematical Society 37: 81-89. MR 0015748, 1945.

[13] N. Levanon, E. Mozeson, Radar Signals, New York, USA: Wiley, 2004.

[14] M.Greco, P. Stinco, F.Gini, A. Farina, Cramér-Rao bounds and TX-RX selection in a multistatic scenario, Proc. of 2010 IEEE Radar Conference, Washington, DC, 2010.

[15] P. Stinco, M. Greco, F. Gini and A. Farina, Sensor selection in PCL radar systems based on bistatic PCRLB, Proc. Advances in Radar and Remote Sensing (TyWRRS), 2012 Tyrrhenian Workshop on, Naples, 2012.

[16] I. Bradaric, G.T. Capraro and M.C. Wicks, Sensor placement for improved target resolution in distributed radar systems, Proc. IEEE Radar Conference, Rome, 2008.

[17] Javier Rosado Sanz, M. Pilar Jarabo Amores, David Anastasio de la Mata Moya, Pedro José Gómez del Hoyo, Nerea del Rey Maestre. Broadband Modified-Circle-Shape Patch Antenna with H-apperture feeding for a Passive Radar Array. Aerospace Science and Technology (Elsevier). Under review.

[18] J. Rosado-Sanz and et al., Advantages of non-uniform linear arrays based on COTS elements in passive radar applications, in 22nd Int. Microwave and Radar Conf., 2018, pp. 199-203.

[19] C. Moscardini and et al., Spatial adaptive processing for passive bistatic radar, in IEEE RadarConf., vol. 1, 2014, pp. 1061-1066.

[20] Aster Data [https://terra.nasa.gov/data/aster-data]. Last accessed: June 2019.

[21] R. Cardinali, F. Colone, C. Ferretti, and P. Lombardo, Comparison of clutter and multipath cancellation techniques for passive radar, in IEEE Radar Conf., vol. 1, 2007, pp. 469-474.